NON-LINEAR SECTIONAL ANALYSIS OF CONCRETE ENCASED STEEL STUB COLUMN SUBJECTED TO AXIAL LOAD

Tugas H. Putra[a], Bambang Piscesa[b], Hidajat Sugihardjo[b]

Abstract: This paper presents a numerical parametric study of Concrete Encased Steel Column (CESC) due to centrically and eccentrically axial load. To model the confining pressure of rebar and steel profile, modified Mander's equations were used. The non-linear sectional analysis was performed using the fiber-based method. The CESC section was discretized using Netgen 2D meshing algorithm. The developed CESC model was validated using the available test results in the literature. After the model was validated, parametric studies were conducted to investigate the behaviors of CESC with different concrete compression strength, confinement bar diameter, and confining distance. The parametric studies found that the columns with higher concrete compression strength tend to have higher axial and flexural capacity but reduce the overall ductility. Increasing the confinement bar diameter slightly increases the axial and flexural capacity and ductility. On the other hand, utilizing tighter confinement space resulted in higher ductility but with insignificant increase in axial and flexural capacity.

Keywords: *Composite structures, concrete encased steel column, fiber-based method, steel-confined concrete, region partition*

Submitted: 08 February 2023; Revised: 24 May 2023; Accepted: 14 June 2023

INTRODUCTION

In the present day, the optimization of building area has become a crucial aspect in construction, leading to a significant demand for reducing the sectional area of the structural column. This can be achieved through increasing the concrete compressive strength and adding the amount of longitudinal reinforcement in concrete columns. However, it must be noted that this method may negatively impact the building's ductility by causing an increase in column brittleness.

Concrete Encased Steel Column (CESC) is a structural element that consists of a steel column encased by a layer of concrete. This type of column provides a combination of the strength and ductility of steel with the fire resistance and mass of concrete, making it a popular choice for many construction projects, especially in seismic zones. Under severe flexural loads, the concrete cover cracks resulting in reduced stiffness, but the steel core provides shear capacity and ductility resistance to subsequent cycles of overload [1]. The concrete material in CESC provides fire resistance and provides support to the steel profile to prevent buckling, also provides protection to the steel column against fire[2] and corrosion[3]. Additionally, the steel profile restrains the concrete core, enabling the concrete core to manage larger axial loads and deformations. Proper restraint is a crucial factor in columns to provide satisfactory plastic hinge rotational capacity.

The maximum strength and behavior of composite columns made of concrete encased steel was determined by [4]. The effects of confinement from both traditional reinforcing bars and structural steel were considered by this method. Three distinct levels of concrete confinement, unconfined, partially confined, and highly confined, were identified by the method. A fiber-based [5] and 3D Nonlinear finite element [6] investigation was carried out to analyses the inelastic behaviors of steel, concrete, longitudinal and transverse reinforcement bars as well as the effect of concrete confinement of the concrete encased steel composite columns, wherein the CESC cross-section was discretized into interconnected sub-elements. Nonetheless, studies are limited to the use of rigid rectangular nets, resulting in a limited area that is less representative of the analysis.

In AISC 360-16 [7], the utilization of specific composite columns, particularly CESC, is limited to the minimum of steel and longitudinal reinforcing cross-sectional area, respectively, of 1% and 0.4% of the total composite column cross-sectional area. In Eurocode-4 [8], the ratio of longitudinal reinforcement is not allowed to exceed 6% of the concrete cross-sectional area. The contribution ratio of steel, δ, must be between 0.2 and 0.9 of the total axial capacity of the cross-section. The ratio between the height and width of the composite column cross-section must be between 0.2 and 5.0. The utilization of high-quality materials such as concrete and steel is limited by both provisions. This is due to the use of high-grade concrete, steel cross-section, and steel reinforcement can result in the brittle behavior of the columns. Taking this into consideration, the behavior of CESC was thoroughly examined in this study.

RESEARCH SIGNIFICANCE

This paper investigates the performance of Concrete Encased Steel Column due to centrically axial load under different concrete strength, confinement bar diameter, and confining spacing. Nonlinear sectional analysis was conducted using the fiber-based method with different confining pressure for unconfined, partially confined and highly confined concrete section. The model was verified with existing experimental data available in the literature. Axial ductility and curvature ductility were used for ductility measurement of the CESC models.

METHODOLOGY

The research methodology in this paper is divided into four stages which are: 1) Collecting specimen data of CESC from previous research[5]. 2) Determine area concrete that influenced by confinement bar and steel profile. 3) Proposing a new modeling method of CESC highly confined concrete due to presence of steel profiles and

[a] Master Student in the Civil Engineering Department, Institut Teknologi Sepuluh Nopember, ITS Campus, Sukolilo, Surabaya 60111, Indonesia
[b] Lecturer in the Civil Engineering Department, Institut Teknologi Sepuluh Nopember, ITS Campus, Sukolilo, Surabaya 60111, Indonesia. Corresponding author email address: piscesa@ce.its.ac.id

longitudinal bar using fiber-based method. 4) Evaluating the behaviors for each CESCs specimen. 5) parametric study was conducted on each specimen to obtain the behavior of CESC.

A. FIBER SECTION ANALYSIS

The method of "fiber section analysis" is a computationally demanding technique for calculating the cross-sectional strength and stiffness of member cross-sections, which circumvents some of the inherent simplifying assumptions in the design models of AISC 360-16 and Eurocode-4. In the fiber method, the cross-section is discretized into numerous small regions where the constitutive relationships are based on uniaxial stress-strain models and each region represents a fiber of material running longitudinally along the member [9]. Figure 1 shows that each fiber assigned as a different constitutive model representing the structural steel, reinforcement steel bar, unconfined concrete, partially confined concrete, and highly confined concrete. To ensure complete compatibility between the steel and concrete components of a composite cross-section, the method assumes that plane sections maintain their plane shape.

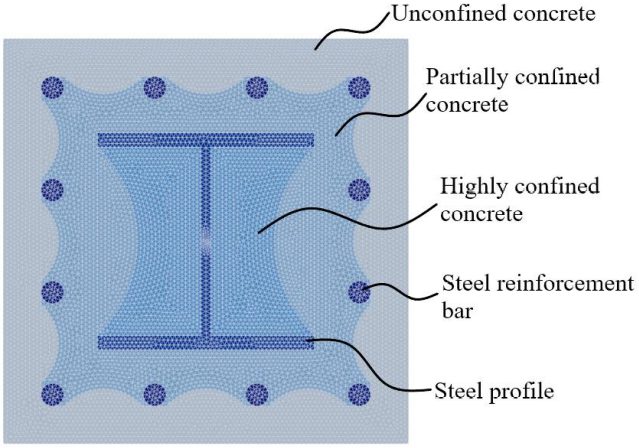

Figure 1 Fiber discretization of Concrete Encased Steel Column

The axial force (P), and bending moment (M_{xx} and M_{yy}) of the cross-section can be calculated as follows:

$$P = \sum_{i=1}^{n_{ele}} \sigma_i A \tag{1}$$

$$M_{xx} = \sum_{i=1}^{n_{ele}} \sigma_i A_i \left(x_i - \bar{x} \right) \tag{2}$$

$$M_{yy} = \sum_{i=1}^{n_{ele}} \sigma_i A_i \left(y_i - \bar{y} \right) \tag{3}$$

B. CONSTITUTIVE MODEL OF MATERIALS

The constitutive model for concrete material was based on the Attard and Setunge model [10] which works well with concrete compressive strength from 20 to 130 MPa. The model operates by computing the stress for a given axial strain. The general expression of the relationship between stress and strain is provided by:

$$Y = \frac{AX + BX^2}{1 + CX + DX^2} \tag{4}$$

Where the values of Y and X are determined by the following equation:

$$Y = \frac{f}{f_o}, X = \frac{\varepsilon}{\varepsilon_o}, \forall X \geq 0, and 0 \leq Y \leq 1 \tag{5}$$

For the axial peak stress for unconfined and confined concrete (f), can be expressed as:

$$\frac{f}{f_o} = \left(\frac{f_r}{f_t} + 1 \right)^k \tag{6}$$

$$k = 1.25 \left[1 + 0.062 \frac{f_r}{f_c^{'}} \right] \left(f_c^{'} \right)^{-0.21} \tag{7}$$

For unconfined concrete, the lateral confinement stress ($f_r = 0$), thus the maximum concrete unconfined strength (f_o) is obtained from a standard cylinder specimen test.

For partially confined concrete, the lateral confinement stress f_{lt}, determined by balancing the tensile forces with the confining pressure times the length of the confined section and the pitch spacing of the transversal rebar [11] (see Figure 2), the expression for partially confined concrete can be expressed as:

$$f_{lt} = \frac{A_{s\,x,y}}{s\,b} \sigma_{yt} \tag{8}$$

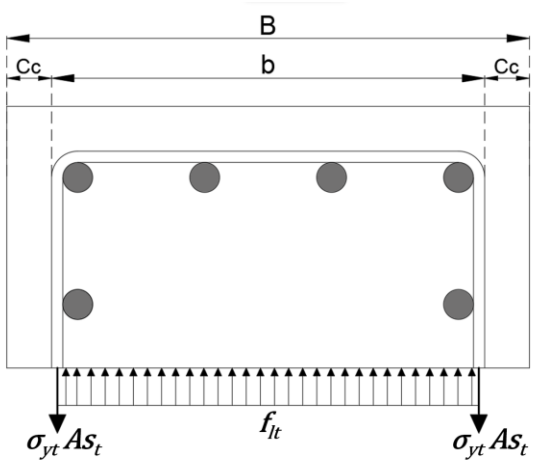

Figure 2 Confinement pressure of partially confined concrete by transversal rebar

For highly confined concrete, the lateral confinement stress (f_{lt}), determined by balancing the ultimate moment of the steel profile's flange (M_u), and plastic moment at the edge of the flange (M_p). [11] (see Figure 2), the expression for highly confined concrete can be expressed as:

$$M_u = M_p \tag{9}$$

$$\frac{0.5 b_f^2 f_{ls}}{2} = \frac{{t_f}^2 \sigma_{s\theta}}{6} \tag{10}$$

Thus, the compressive stress resulting from the steel profile wing f_{ls} is obtained.

$$f_{ls} = \frac{2{t_f}^2 \sigma_{s\theta}}{3 b_f^2} \tag{11}$$

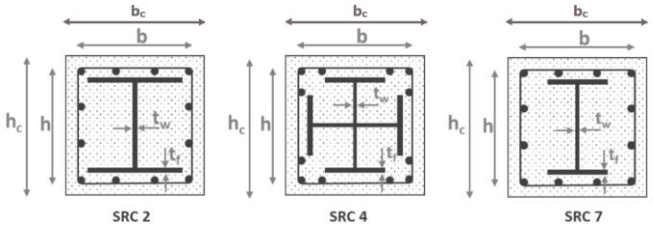

Figure 6 Specimen verification model of CESC Sections.

Table 1 Geometrical and material properties of composite stub columns.

Specimen	Cross Section (mm)	Structural Steel	Longitudinal Bar (mm)	Confining Bar (mm)	f'_c (MPa)	f_{yr} (MPa)	f_{ys} (MPa)	P_u (kN)
SRC 2	280 x 280	H 150x150x7x10	12-D16	ϕ7-75	28.1	350	296	4228
SRC 4	280 x 280	C 175x90x5x8	12-D16	ϕ7-140	29.8	350	345	4441
SRC 7	280 x 280	IWF 150x75x5x7	12-D16	ϕ7-140	29.5	350	303	3788

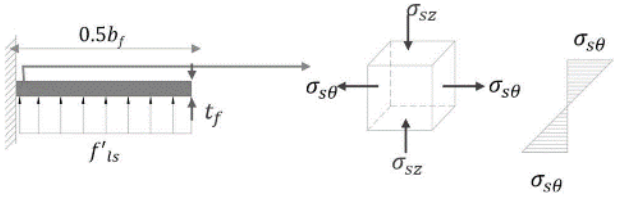

Figure 3 Confinement pressure of partially confined concrete by steel profile flange

When the CESC column is subjected to axial compression the longitudinal bars undergo local buckling that decrease the load carrying capacity and ductility, as observed in the test of reinforcing bars [12]. A simple constitutive stress-strain model proposed considering the inelastic buckling of the longitudinal bars under compression [4]. The longitudinal bar under compression will reach the yield strength with a yield plateau. It is assumed that the reinforcement bar will buckle and lose its strength due to the spalling of the concrete cover when the concrete cover reaches its peak strength. The bar's stress commences its deterioration once the axial strain of the bar reaches the strain value (εc_0), The stress of the reinforcement will decrease to 20% of its yield strength and remain constant thereafter the yield strength is assumed when the axial strain reaches four times the (εc_o).

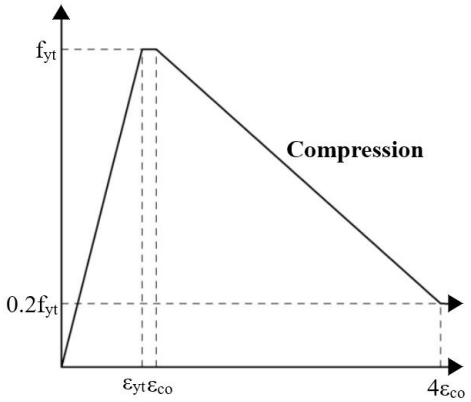

Figure 4 Stress–strain relation for longitudinal reinforcing bar in compression

The same stress-strain constitutive model that is adopted for the longitudinal bars is assumed for the structural steel section. Local buckling of the steel section elements, particularly at the flange, is likely to occur after partially confined concrete crushing. Hence, degradation of stress is assumed after the axial strain reaches the (εc_p), indicating partial concrete crushing. A post-peak strength of 20% of the yield strength is assumed when the axial strain reaches four times the (εc_p).

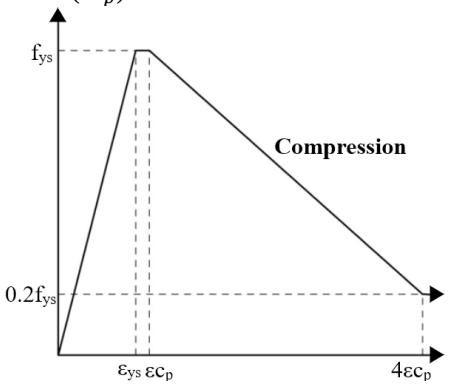

Figure 5 Stress–strain relation for longitudinal reinforcing bar in compression

C. FIBER SECTION MODEL VERIFICATION AND PARAMETRIC STUDY

The comparison between the analytical predictions of the axial compressive behavior and capacity of the composite CESC and the experimental results is conducted. Three series of tests that are relevant to the purpose of the study are taken into consideration[4]. SRC2, SRC4, and SRC7 respectively investigated, Figure 6 shows the geometric configuration of the CESC and Table 1 shows geometrical and material properties of composite stub columns. The auxiliary program used to model the geometrical cross-section of the shear wall structure was SALOME 9.3.0. Monotonic loading was conducted at the specimens due to centrally and eccentrically load, using method that previously used.[13], [14], [15].

A parametric study was conducted on each specimen to obtain the behavior of the CESC in response to variations in concrete compressive strength, reinforcement spacing, and stirrup diameter as shown in Table 2.

Table 2 Variation CESC model with different properties

Variations	Confining Spacing (mm)	f'_c (MPa)	Confining Bar (mm)	Confining Pressure (MPa)
Var-1	280	30	8	0.082
Var-2	140	30	8	0.458
Var-3	75	30	8	1.321
Var-4	35	30	8	3.104
Var-5	140	45	8	0.458
Var-6	140	60	8	0.458
Var-7	140	30	6	0.255
Var-8	140	30	10	0.724

RESULTS AND DISCUSSIONS

Three CESC specimens will be evaluated using non-linear fiber-based analysis. The relationship that is being investigated and compared is localized only to the axial-strain analysis. The specimen geometry is reported in Table 1, and the concrete compressive strength was varied for each case. The specimen is identified as SRC2, SRC4, and SRC7 which represents the CESC with H-Shaped, Cruciform Shaped, and I-Shaped steel column, the results shows that the ratio of P_{exp} / P_{max} closer to 1, which is shows that the CESC Proposed model was suitable to use.

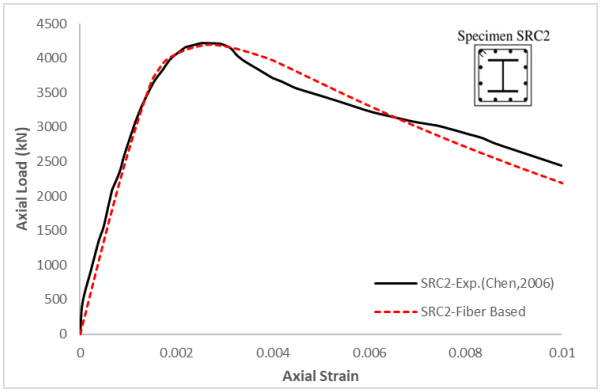

(a)

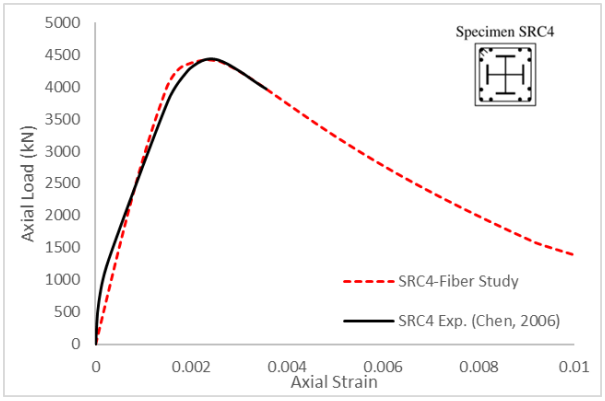

(b)

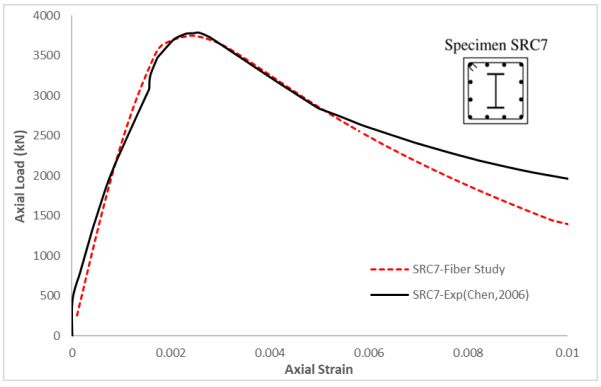

(c)

Figure 7 Comparison of the proposed model with the test result (a) SRC2, (b) SRC4, (c) SRC7

Figure 7 shows the comparison of the proposed model with the available test results for SRC2, SRC4, and SRC7 columns. As shown in Figure 7, the performance of the proposed model was sufficient to predict the behavior of the CESC with varying initial conditions.

Table 2 Variation CESC model with different properties

Specimens	Experimental data		Fiber Based Model		P_{exp} / P_{fiber}
	P_{max} (kN)	ε_{max}	P_{max} (kN)	ε_{max}	
SRC2	4228	0.0024	4195	0.0027	1.007
SRC4	4441	0.0025	4416	0.0023	1.006
SRC7	3788	0.0026	3747	0.0024	1.011

Table 2 shows that the performance of the proposed model was sufficient to predict the behavior of the CESC with varying initial conditions.

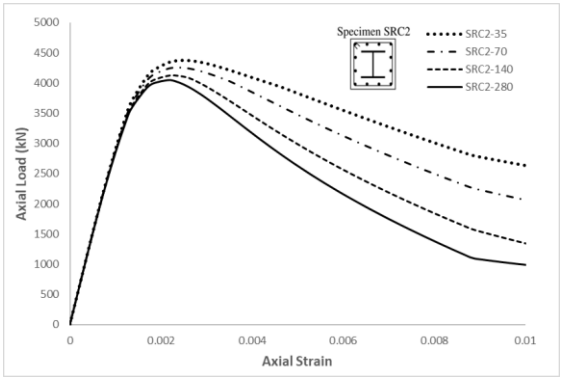

(a)

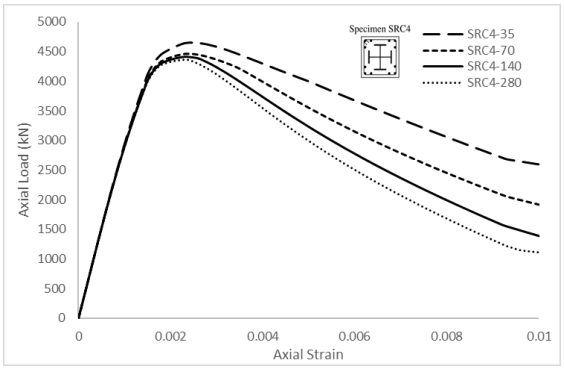

(b)

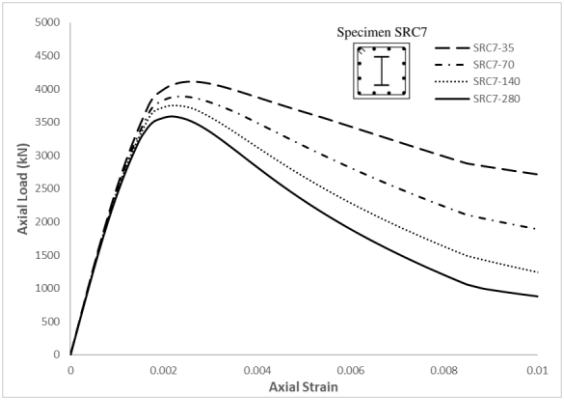

(c)

Figure 8 Effect of tie spacing on axial load–strain curves: (a) H-shaped steel section; (b) cross-shaped steel section; (c) I-Shaped Section

Figure 8 and Table 2 present the parametric study of specimens SRC2, SRC4, and SRC7 with stirrup spacings of 280mm, 140mm, 70mm, and 35mm, respectively. It can be concluded that the transverse stirrup spacing affects the ultimate axial force and ductility behavior of the column,

and shows that as the stirrup spacing becomes closer, the ultimate axial force that can be provided increases and the column becomes more ductile.

Table 2 Variation CESC model with different transverse stirrup spacing.

Specimens	P_{max} (kN)	0.85 P_{max} (kN)	ε_{max}	0.85 ε_{max}	DI
SRC2 Var-1	4377	3721	0.0025	0.0054	2.16
SRC2 Var-2	4251	3614	0.0024	0.0046	1.92
SRC2 Var-3	4123	3505	0.0022	0.0039	1.77
SRC2 Var-4	4054	3466	0.0022	0.0035	1.59
SRC4 Var-1	4656	3957	0.0024	0.0051	2.13
SRC4 Var-2	4465	3795	0.0024	0.0045	1.88
SRC4 Var-3	4416	3756	0.0023	0.0039	1.70
SRC4 Var-4	4366	3711	0.0023	0.0037	1.61
SRC7 Var-1	4111	3495	0.0026	0.0057	2.19
SRC7 Var-2	3890	3307	0.0024	0.0045	1.88
SRC7 Var-3	3752	3190	0.0022	0.0039	1.77
SRC7 Var-4	3590	3051	0.0022	0.0036	1.64

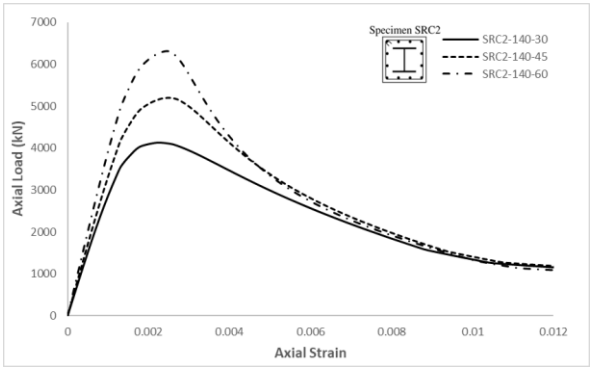

(a)

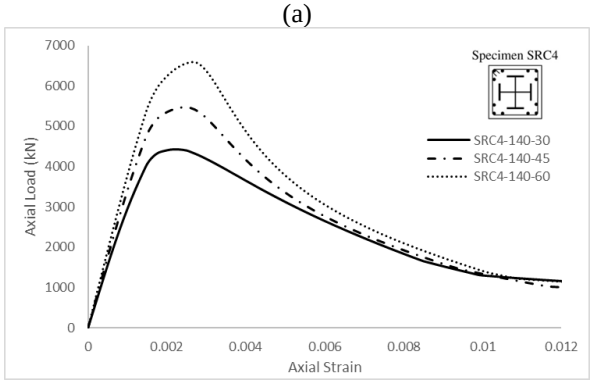

(b)

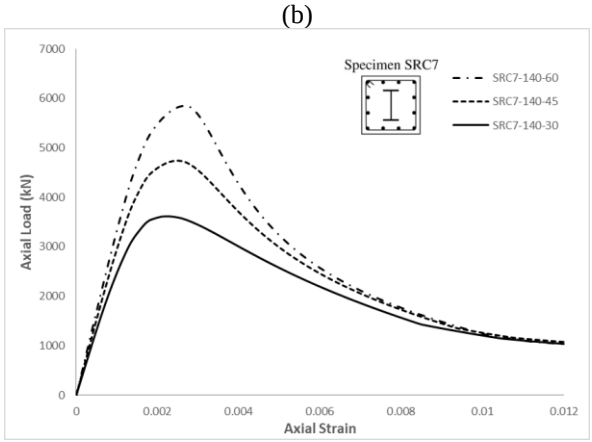

(c)

Figure 9 Effect of concrete compressive strength on axial load–strain curves: (a) H-shaped steel section; (b) cross-shaped steel section; (c) I-Shaped Section

Figure 9 and Table 3 present the parametric study of specimens SRC2, SRC4, and SRC7 with different concrete compressive strength from 30 MPa, 45 MPa, and 60 MPa, respectively. It can be concluded that the concrete compressive strength affects the ultimate axial force and ductility behavior of the column and shows that as the concrete compressive strength becomes higher, the ultimate axial force that can be provided increases, making it more susceptible to brittle failure.

Table 3 Variation CESC model with different concrete compressive strength

Specimens	P_{max} (kN)	0.85 P_{max} (kN)	ε_{max}	0.85 ε_{max}	DI
SRC2 Var-2	4123	3504	0.0023	0.0039	1.70
SRC2 Var-5	5205	4424	0.0025	0.0036	1.44
SRC2 Var-6	6305	5359	0.0025	0.0033	1.32
SRC4 Var-2	4419	3756	0.0022	0.0038	1.73
SRC4 Var-5	5463	4644	0.0025	0.0035	1.40
SRC4 Var-6	6580	5593	0.0027	0.0035	1.30
SRC7 Var-2	3613	3071	0.0023	0.0038	1.65
SRC7 Var-5	4736	4026	0.0025	0.0036	1.44
SRC7 Var-6	5857	4978	0.0027	0.0035	1.30

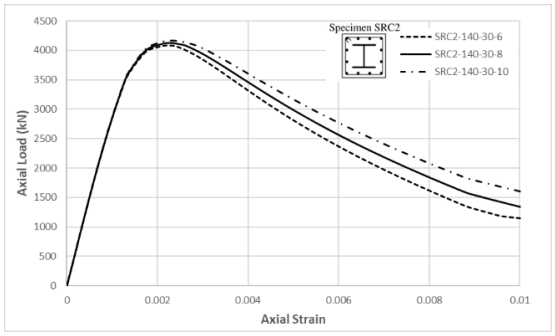

(a)

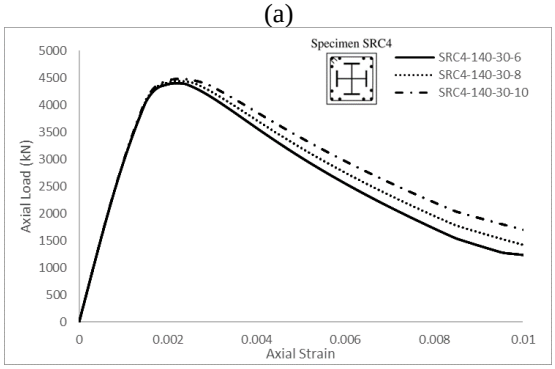

(b)

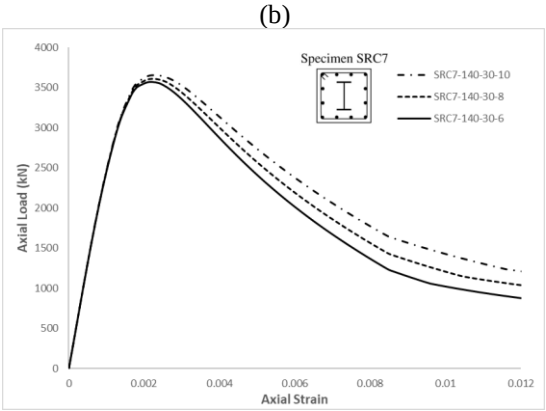

(c)

Figure 10 Effect of transversal rebar diameter on axial load–strain curves: (a) H-shaped steel section; (b) cross-shaped steel section; (c) I-Shaped Section

Figure 10 and Table 4 present the parametric study of specimens SRC2, SRC4, and SRC7 with different transversal rebar diameter from 6 mm, 8 mm, and 10 mm, respectively. It can be concluded that the transversal rebar diameter affects the ultimate axial force and ductility behavior of the column and shows that as the transversal rebar diameter higher, the ultimate axial force that can be provided increases, but the column becomes more ductile.

Table 4 Variation CESC model with different concrete compressive strength

Specimens	P_{max} (kN)	0.85 P_{max} (kN)	ε_{max}	0.85 ε_{max}	DI
SRC2 Var-2	4123	3505	0.0023	0.0039	1.70
SRC2 Var-7	4087	3475	0.0022	0.0037	1.68
SRC2 Var-8	4167	3542	0.0023	0.0041	1.78
SRC4 Var-2	4436	3771	0.0022	0.0039	1.77
SRC4 Var-7	4405	3744	0.0022	0.0037	1.68
SRC4 Var-8	4475	3804	0.0023	0.0041	1.78
SRC7 Var-2	3613	3071	0.0022	0.0037	1.77
SRC7 Var-7	3575	3038	0.0022	0.0039	1.68
SRC7 Var-8	3660	3659	0.0023	0.0041	1.78

CONCLUSIONS

This paper investigates the performance of Concrete Encased Steel Column due to centrically axial load under different concrete strength, confinement bar diameter, and confining spacing. Nonlinear sectional analysis was conducted using the fiber-based method with different confining pressure for unconfined, partially confined and highly confined concrete section.

From the study, The CESC constitutive method with various steel section profiles proposed can provide predictions of peak axial capacity, axial force-strain graphs that resemble existing experimental results.

Parametric study was conducted to determine the behavior of CESC against concrete quality, spacing of transverse reinforcement, and diameter of transverse reinforcement that concluded the following: 1) An increase in concrete quality can increase the ultimate axial capacity of CESC but decrease its ductility.2) The spacing of transverse reinforcement can increase the ultimate axial capacity of CESC because the concrete is restrained by the reinforcement. This restraint can also increase the ductility of the CESC column. 3) A larger diameter of transverse reinforcement can increase the restraint factor on partially restrained concrete core. Thus, it can increase the ultimate axial capacity and ductility of the column.

REFERENCES

[1] N. E. Shanmugam and B. Lakshmi, "State of the art report on steel-concrete composite columns," Journal of Constructional Steel Research, vol. 57, no. 10, pp. 1041–1080, 2001, doi: 10.1016/S0143-974X (01)00021-9.

[2] S. Li, J. Y. R. Liew, and M. X. Xiong, "Prediction of fire resistance of concrete encased steel composite columns using artificial neural network," Engineering Structures, vol. 245, Oct. 2021, doi: 10.1016/j.engstruct.2021.112877.

[3] Y. Zhao, D. Zhang, S. Shen, and T. Ueda, "Axial loading capacity of concrete-jacketed RC columns with pre- and post-corrosion damage," Structural Concrete, vol. 17, no. 3, pp. 355–364, Sep. 2016, doi: 10.1002/suco.201400113.

[4] C. C. Chen and N. J. Lin, "Analytical model for predicting axial capacity and behavior of concrete encased steel composite stub columns," Journal of Constructional Steel Research, vol. 62, no. 5, pp. 424–433, May 2006, doi: 10.1016/j.jcsr.2005.04.021.

[5] V. S. Ky, S. Tangaramvong, and T. Thepchatri, "Inelastic analysis for the post-collapse behavior of concrete encased steel composite columns under axial compression," Steel and Composite Structures, vol. 19, no. 5, pp. 1237–1258, 2015, doi: 10.12989/scs.2015.19.5.1237.

[6] B. S. El-Tawil, A. Member, and G. G. Deierlein, "Strength and ductility of concrete encased composite columns.", vol. 125, no. 9, pp. 1009-1919, Sep.1999, doi: 10.1061/(ASCE)0733-9445(1999)125:9(1009)

[7] A. I. S. Construction, Specification for structural steel buildings supersedes the specification for structural steel buildings dated and all previous versions approved by the committee on specifications, Chicago: American Institute of Construction, 2016.

[8] N. Europeenne, European standard eurocode 4: Design of composite steel and concrete structures-part 1-1: General rules and rules for buildings, Brussels: CEN, 2004.

[9] D. L. Logan, A first course in the finite element method CL engineering, California: Brooks/Cole, 2002.

[10] M. M. Attard, S. Setunge "Stress-strain relationship of confined and unconfined concrete" ACI Materials Journals, vol. 93, no. 5, pp. 432-442, 1996.

[11] J. B. Mander, M. J. N. Priestley, and R. Park, "Theoretical stress-strain model for confined concrete.", vol. 114, no. 8, doi:10.1061/(ASCE)07339445(1988)114:8(1804)

[12] O. Bayrak and S. A. Sheikh, "Plastic hinge analysis," pp. 1092, Journal of Structural Engineering, vol. 127, no. 9, pp. 1092-1100, 2001.

[13] T. Fujimoto, A. Mukai, I. Nishiyama, and K. Sakino, "Behavior of eccentrically loaded concrete-filled Steel tubular columns", Journal of Structural Engineering, vol. 130, no. 2, pp. 203-212, 2004. doi: 10.1061/ASCE0733-94452004130:2203.

[14] K. Sakino, H. Nakahara, S. Morino, and I. Nishiyama, "Behavior of centrally loaded concrete-filled steel-tube short columns", Journal of Structural Engineering, vol. 130, no. 2, pp. 180-188, 2004. doi: 10.1061/ASCE0733-94452004130:2180.

[15] B. Piscesa, M. M. Attard, P. Suprobo, and A. K. Samani, "Investigation on the fiber-based approach to estimate the axial load carrying capacity of the circular concrete filled steel tube (CFST)," IOP Conference Series: Materials Science and Engineering, vol. 267, no. 1, 2017, doi: 10.1088/1757-899X/267/1/012017.

LIST OF NOTATIONS

A is the surface area of every CESC region (mm^2)
A_{st} is the area of steel rebar (mm^2)
b is the overall width of the CESC (mm)
b_f is the width of the steel column (mm)
c_c is the cover thickness of the column existing (mm)
c_j is the cover thickness of the concrete jacket (mm)
d_{bc} is the diameter and number of the longitudinal bar for the core section (mm)
DI is ductility index of CESC columns.
f'_c is the compressive strength of the concrete (MPa)
f_{lt} is the lateral confinement stress of the transverse rebar (MPa)
f_{ls} is the lateral confinement stress of the steel profile (MPa)
f_o is the lateral confinement stress of the unconfined concrete (MPa)
f_r is the lateral confinement stress of the column (MPa)
f_{yr} is the yield strength of the steel rebar (MPa)
f_{ys} is the yield strength of the steel profile (MPa)
k is the effectiveness of confinement
Mu is the ultimate moment of the steel profile's flange (kN.m)
Mp is the plastic moment at the edge of the flange (kN.m)
M_{xx} is the bending moment capacity of CESC in x-dir (kN.m)
M_{yy} is the bending moment capacity of CESC in y-dir (kN.m)
t_f is the thickness of the steel profile flange (mm)
t_w is the thickness of the steel profile web (mm)
P_{max} is the axial capacity of CESC (kN)
$\sigma_{s\theta}$ is the tensile yield stress of steel profile (MPa)
σ_{yt} is the hoop stress of steel rebar in yeld conditions (MPa)
ε_{Max} is the strain of the CESC at P_{max}